INT. J. NUM. METH. HEAT FLUID FLOW, VOL. 3, 305–318 (1993)

FINITE ELEMENT ANALYSIS OF THE EFFECT OF RADIUS RATIO ON NATURAL CONVECTION IN AN ANNULAR CAVITY

B. V. K. SATYA SAI*, K. N. SEETHARAMU* AND P. A. ASWATHA NARAYANA†

Department of Mechanical Engineering and Department of Applied Mechanics† Indian Institute of Technology, Madras 600 036, India*

AND

J. N. REDDY

Department of Mechanical Engineering, Texas A&M University, College Station, Texas 77843, USA

ABSTRACT

A finite element method based on the Eulerian velocity correction method has been used to analyse the laminar natural convection in an annular cavity. Unsteady, incompressible, axisymmetric Navier–Stokes equations have been made use of. Different radius ratios of the annular cavity have been considered to investigate the effect of the radius of curvature on the heat transfer coefficient.

KEY WORDS Velocity correction method Laminar natural convection Pressure Poisson equation Radius ratio Nusselt number distribution

NOMENCLATURE

D	height of the annular cavity
Gr	Grashof number based on the width of the cavity $=\dfrac{(r_o-r_i)^3 g\beta(T_i-T_o)}{\nu^2}$
L_{ref}	reference length (r_0-r_i)
$\overline{Nu}$	average Nusselt number
Nu_{max}	maximum Nusselt number
Pe	Peclet number $=Re\cdot Pr$
Pr	Prandtl number
Ra	Rayleigh number $=Gr\cdot Pr$
Re	Reynolds number based on U^{ref} and L^{ref}
r_i	inner radius of the annular cavity
r_o	outer radius of the annular cavity
T_i	inner wall temperature
T_o	outer wall temperature
U_1	vertical component of velocity
U_2	radial component of velocity

Greek notations

β	thermal expansion coefficient
λ	radius ratio (r_i/r_o)
$\delta_{i,j}$	Kronecker delta (equal to 0 if $i\neq j$ and 1 if $i=j$)
ν	kinematic viscosity

INTRODUCTION

The determination of buoyancy-driven flows in an enclosed cavity has many applications of which the most widely known is that of double glazing[1]. The natural convection heat transfer in an annular cavity also falls in this category. It finds applications in areas like nuclear reactors,

0961–5539/93/040305–14$2.00

Received June 1992
Revised December 1992

where there would be an annular gap between the core and the surrounding pressure vessel. Another example is the apparatus commonly used for measuring the thermal conductivity of a fluid in which an electrically heated wire is mounted on the axis of a cylinder.

The experimental results on annular cavities are very few and are applicable for only a limited and specified values of aspect ratio (A) and radius ratio ($1/\lambda$), for example Nagendra *et al.*[2]. The effect of radius ratio and aspect ratio on natural convection heat transfer in an annular cavity in which a constant heat flux is maintained at the inner wall has been investigated by Keyhani *et al.*[3], Bhushan *et al.*[4], Khan *et al.*[5] and Fang and Paraschivoiu[6]. But the literature is limited for the case of an annular cavity with constant wall temperatures (wall heated by condensation process). One of the earlier works of this nature is that of de Vahl Davis and Thomas[7]. They presented numerical results for laminar axisymmetric natural convection in a vertical annulus with aspect ratios 5 to 20 and radius ratios (r_o/r_i) 1 to 4. They found that the mean heat transfer coefficient at the inner wall was found to decrease with an increase in aspect ratio and increase with an increase of radius ratio. Wu-Shung Fu *et al.*[8] conducted a study of the transient natural convection in an annular cavity for a single radius ratio. They adopted the numerical method of SIMPLE-R with power law scheme. They came out with a very useful observation that the phenomenon of the position of the maximum stream function moving from near the inner wall region to near the outer wall region is different from that in a square enclosure. Also it was observed that the low temperature region is much larger than that in the square cavity. Le Quere and Pecheux[9] reported that tall annular flows are unstable with respect to non axisymmetric disturbances for larger values of radius ratio. Farouk *et al.*[10] used the stream function–vorticity form of the Navier–Stokes equations for a similar study. They considered aspect ratios up to 5 and did not take any radius ratio beyond 3 in view of the findings of Reference 9. In addition to finding out that the heat transfer is maximum when the aspect ratio is 1, Farouk *et al.*[10] also concluded that the effectiveness of transport of heat by natural convection is diminished continuously as the ratio ($1/\lambda$) is increased for a particular aspect ratio. This is apparently in contradiction with the results of de Vahl Davis and Thomas[7]. Farouk *et al.* attribute the discrepancy to the difference in the choice of the parameters used to present the heat transfer results. While de Vahl Davis and Thomas used the Nusselt numbers, Farouk *et al.* have used the expression for the equivalent thermal conductivity. More recently Woon-shing Yeung[11] carried out a semi-analytical analysis for the free convection in a closed vertical annulus with isothermal walls and insulated top and bottom surfaces using the conduction layer approximate method (CLAM). This method is based on the premise that individual thin boundary layers develop along the vertical walls in the so-called boundary layer regime, and as such the applicability of this method is restricted to higher Rayleigh number range only. Thus there is a general lack of literature on the effect of radius ratio on the distribution of Nusselt number over the hot and cold walls.

In the present study, the finite element method based on Euler's velocity correction method has been used to find the effect of radius ratio on the heat transfer characteristics of an annular cavity of aspect ratio 1. The two vertical walls are maintained at different temperatures and the horizontal walls are kept insulated. A fluid of Prandtl number 0.71 has been considered in the Rayleigh number range of 10^9 to 10^6 which falls in the laminar regime. The temperature and velocity fields and the Nusselt number variation along both hot and cold walls have been investigated for different Rayleigh numbers in the above range.

GOVERNING EQUATIONS

The non-dimensionalized axisymmetric laminar equations for the case of natural convection are given below in indicial notation.

Continuity equation:

$$\frac{1}{X_2}(X_2 U_i)_{,i}=0 \tag{1}$$

Momentum equation:

$$U_{i,\tau}=-P_{,i}-U_j U_{i,j}+\frac{1}{ReX_2}(X_2(U_{i,j}+U_{j,i}))_{,j}-\delta_{i,2}2\frac{U_i}{ReX_2^2}+\delta_{i,1}\frac{Gr}{Re^2}T \tag{2}$$

Energy equation:

$$T_{,\tau}+U_i T_{,i}=\frac{1}{PeX_2}(X_2 T_{,i})_{,i} \tag{3}$$

All the velocities are non-dimensionalized with a reference velocity U^{ref}. Most of the authors follow a method of non-dimensionalization which gives rise to a $Ra.Pr$ term in the momentum equation in the direction of the gravity field. In the present work Gr/Re^2 term appears in the momentum equation. In order to obtain a direct comparison between the two methods, it is necessary that U_{ref} be chosen in such a way as to give an $Re=1/Pr$. All lengths have been non-dimensionalized with the difference of the inner and outer radii (r_o-r_i). Time is non-dimensionalized using the ratio (L^{ref}/U^{ref}) and temperature with ΔT^{ref} (temperature difference between the hot and cold walls). *Re*, *Gr* and *Pe* are the Reynolds number, Grashof number and Peclet number respectively and are given by:

$$Re=\frac{U^{ref}L^{ref}}{\nu} \tag{4}$$

$$Gr=\frac{L^3 g\beta\Delta T^{ref}}{\nu^2} \tag{5}$$

$$Pe=Re.Pr \tag{6}$$

This type of non-dimensionalization which gives rise to the term Gr/Re^2 has got an advantage in that, (1), (2), (3) can also be used to solve a mixed convection problem wherein both the forced and free convection are equally dominant.

EULERIAN VELOCITY CORRECTION METHOD

In this method the solution is advanced in three steps at each time step. These three steps are calculation of pseudo velocities, evaluation of pressure from the Poisson equation and correction of pseudo velocities to obtain velocities at the next time step.

Calculation of pseudo velocities

The pseudo or fictitious velocities are calculated from (2) by dropping the pressure terms:

$$V_{i,\tau}=-U_j U_{i,j}+\frac{1}{ReX_2}(X_2(U_{i,j}+U_{j,i}))_{,j}-\delta_{i,2}2\frac{U_i}{ReX_2^2}+\delta_{i,1}\frac{Gr}{Re^2}T \tag{7}$$

Using the Euler's explicit scheme to expand the l.h.s. of the above equation in the time domain:

$$V_{i,\tau}=\frac{V_i^{n+1}-U_i^n}{\Delta T^n} \tag{8}$$

Equation (7) can now be written as:

$$\frac{V_i^{n+1}-U_i^n}{\Delta T^n}=-U_jU_{i,j}+\frac{1}{ReX_2}(X_2(U_{i,j}+U_{j,i}))_{,j}-\delta_{i,2}2\frac{U_i}{ReX_2^2}+\delta_{i,1}\frac{Gr}{Re^2}T \tag{9}$$

The above equation is used to calculate the pseudo velocities.

Pressure equation

From (2) and (9) we obtain:

$$U_{i,\tau}-V_{i,\tau}=-P_{,i} \tag{10}$$

Expanding both the time derivatives explicitly and simplifying we get:

$$P_{,i}^{n+1}=\frac{V_i^{n+1}-U_i^{n+1}}{\Delta T^n} \tag{11}$$

Taking the partial derivatives of (11) with respect to X_i and modifying, we arrive at the following pressure Poisson equation:

$$\frac{1}{X_2}(X_2P_{,i}^{n+1})_{,i}=\frac{1}{\Delta\tau^n}\left(\frac{1}{X_2}(X_2V_i^{n+1})_{,i}\right) \tag{12}$$

Velocity correction

The original velocities of the next time step U_i^{n+1} are obtained by correcting the pseudo velocities using the pressure evaluated as shown below:

$$U^{n+1}=V^{n+1}-P_{,i}^{n+1}\,\Delta\tau^n \tag{13}$$

Finally, the temperature is calculated using an explicit form of (3):

$$\frac{T^{n+1}-T^n}{\Delta\tau^n}=-U_iT_{,i}+\frac{1}{PeX_2}(X_2T_{,i})_{,i} \tag{14}$$

The various steps in the solution procedure can be summarized as follows:

(i) start with initial conditions of U^n, V^n and T^n
(ii) find the fictitious velocities V^{n+1} using (9)
(iii) find pressure P^{n+1} using (12)
(iv) find the corrected velocity U^{n+1} using (13)
(v) find T^{n+1} using (14). If transient results are required, then it is necessary to iterate at each time step to get the corrected temperature at that time step. Otherwise repeat the steps (ii) to (v) till the steady state values are obtained.

FINITE ELEMENT FORMULATION

Finite element method based on Galerkin's weighted residual technique has been used to solve the above equations. Linear triangular elements have been used to discretize the solution domain. Various steps involved in the finite element formulation are explained in Reference 12.

The finite element equation for the calculation of fictitious velocities is obtained as:

$$[K_{F1}]\{V_i^{n+1}\}=\{F_{F1}\} \tag{14}$$

where

$$[K_{F1}]=\int_A [N]^T[N]2\Pi X_2\,dA \tag{15}$$

and

$$\{F_{F1}\}=[K_{F1}]\{U_i^n\}-\int_A [N]^T[N]\{U_j^n\}[N]_{,j}\Delta\tau^n 2\Pi X_2\,dA\{U_i^n\}-$$
$$\int_A \Delta\tau^n[N]_{,j}^T\frac{1}{Re}(U_{i,j}^n+U_{j,i}^n)2\Pi X_2\,dA-$$
$$2.\delta_{i,2}\int_A \Delta\tau^n[N]^T\frac{1}{ReX_2^2}[N](U_i^n)2\Pi X_2\,dA+$$
$$\delta_{i,1}\frac{Gr}{Re^2}\int_A \Delta\tau^n[N]^T[N]\{T^n\}2\Pi X_2\,dA \tag{16}$$

The finite element equation for the pressure Poisson equation is given by:

$$[K_{F2}]\{P^{n+1}\}=\{F_{F2}\} \tag{17}$$

where

$$[K_{F2}]=-\int_A [N]_{,i}^T[N]_{,i}2\Pi X_2\,dA \tag{18}$$

$$\{F_{F2}\}=\int_A [N]^T(X_2V_i^{n+1})_{,i}2\Pi\,dA \tag{19}$$

The finite element equation for the velocity correction is obtained as:

$$[K_{F1}]\{U_i^{n+1}\}=\{F_{F3}\} \tag{20}$$

where

$$\{F_{F3}\}=[K_{F1}]\{V_i^{n+1}\}-\int_A \Delta\tau^n[N]^TP_{,i}^{n+1}2\Pi X_2\,dA \tag{21}$$

Equations (14), (17) and (20) are the element matrices which are assembled to get the global matrices.

Similarly the Galerkin technique when applied to the unsteady state energy equation gives:

$$[K_{T1}]\{T^{n+1}\}=\{F_{T1}\} \tag{21}$$

where

$$[K_{T1}]=\int_A [N]^T[N]2\Pi X_2\,dA \tag{22}$$

$$\{F_{T1}\}=[K_{T1}]\{T^n\}-\int_A ([N]^T[N]\{U_i^n\}[N]_{,i}+\frac{1}{Pe}[N]_{,i}^T[N]_{,i})2\Pi X_2\,dA\{T^n\}-$$
$$\frac{1}{Pe}\int_{\Gamma_1}\Delta\tau^n[N]^Tq2\Pi X_2\,d\Gamma-\frac{1}{Pe}\int_{\Gamma_2}\Delta\tau^n[N]^Th(T^n-T^a)2\Pi X_2\,d\Gamma \tag{23}$$

Here only the Poisson equation for pressure is solved from a set of algebraic equations. In all the other steps, mass lumping is done on l.h.s. This simplifies the solution procedure as it results

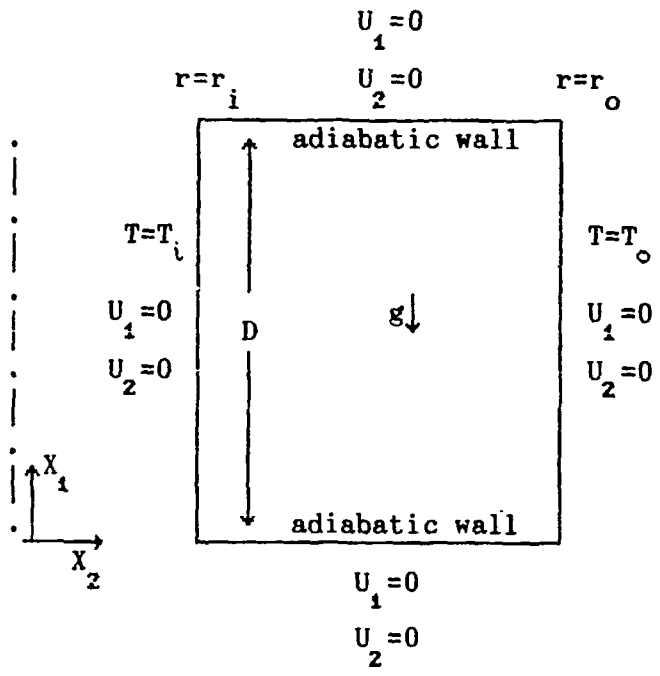

Figure 1 Geometry of the problem considered

in a diagonal matrix on l.h.s. The inverse of a diagonal matrix is nothing but each element replaced by its reciprocal. This enhances the speed of computation. Also the stiffness matrix in the pressure Poisson equation need be assembled only once and only the r.h.s. i.e., the load vector changes at each time step. All these features offset the disadvantages of the explicit scheme and render the algorithm cost effective.

GEOMETRY AND BOUNDARY CONDITIONS

Figure 1 shows the geometry of the annular cavity and the boundary conditions. The inner wall is maintained at a temperature T_i and the outer wall at a temperature T_o, whereas the two horizontal walls are kept insulated. No slip condition prevails on all the four boundaries. In all the cases air with a Prandtl number 0.71 has been considered as the fluid. The aspect ratio $[D/(r_o-r_i)]$ has been taken to be 1.

NUMERICAL RESULTS

The computations were carried out using a non-uniform mesh of 841 nodes and 1568 elements. The domain has been discretized and graded in such a way that we get a very fine mesh near the walls of the cavity and a relatively coarse mesh in the core region. Although the algorithm is a transient one, only the steady state results have been presented for three different radius ratios, namely, $\lambda=0.999$, 0.50 and 0.091 (or $1/\lambda \simeq 1$, 2 and 11).

Figure 2(a,b,c) and *Figure 3(a,b,c)* show the variation of the vertical component of velocity (U_1) and the temperature along horizontal mid-plane of the cavity for $\lambda=0.999$, 0.50 and 0.091 respectively. *Figure 4(a,b,c)* show the Nusselt number variation along the hot wall of the cavity

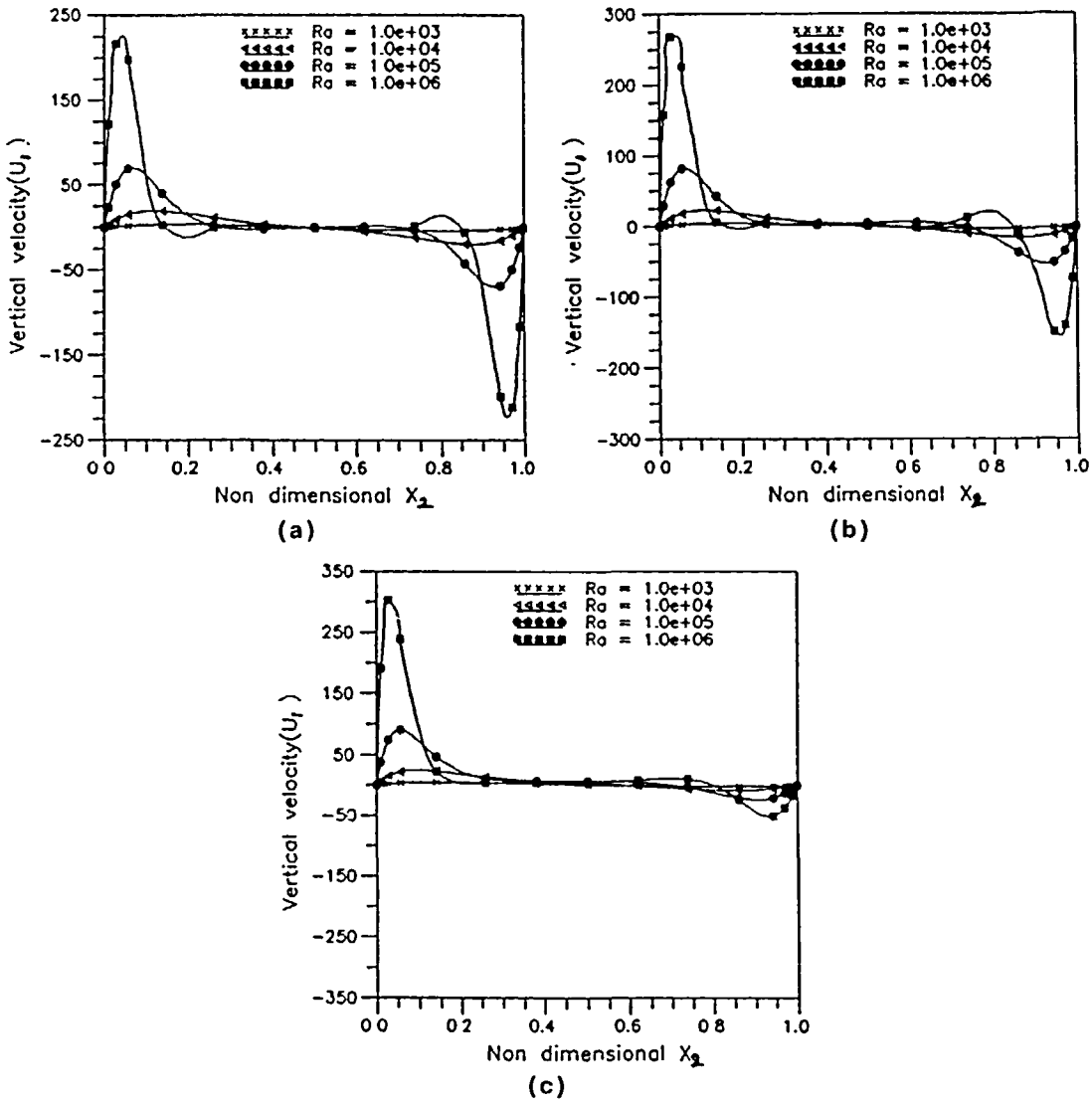

Figure 2 Comparison of the vertical component of velocity along the horizontal mid-plane of the cavity for different Rayleigh numbers: (a) $\lambda=0.999$, (b) $\lambda=0.500$, (c) $\lambda=0.091$

for the same cases mentioned above. In all the three Figures, for the case $\lambda=0.999$, the inner radius, $r_i \gg (r_o - r_i)$ which means that the effect of curvature is almost negligible. The results for this case correspond to a plane cavity problem. This is evident from the close agreement between the present results and the published results[13,14] for a plane cavity as shown in *Tables 1* and *2*. *Table 1* shows a comparison of the maximum vertical component of velocity as obtained in the present investigation with those in References 13 and 14. *Table 2* shows a comparison of the average Nusselt number along the hot wall of the cavity for different Rayleigh numbers for $\lambda=0.999$, with the benchmark solutions of de Vahl Davis[13].

It is observed from *Figures 2(b,c)* and *3(b,c)* that as λ decreases the effect of curvature comes into picture. For $\lambda=0.50$ and 0.091 the vertical component of velocity (U_1) and the temperature

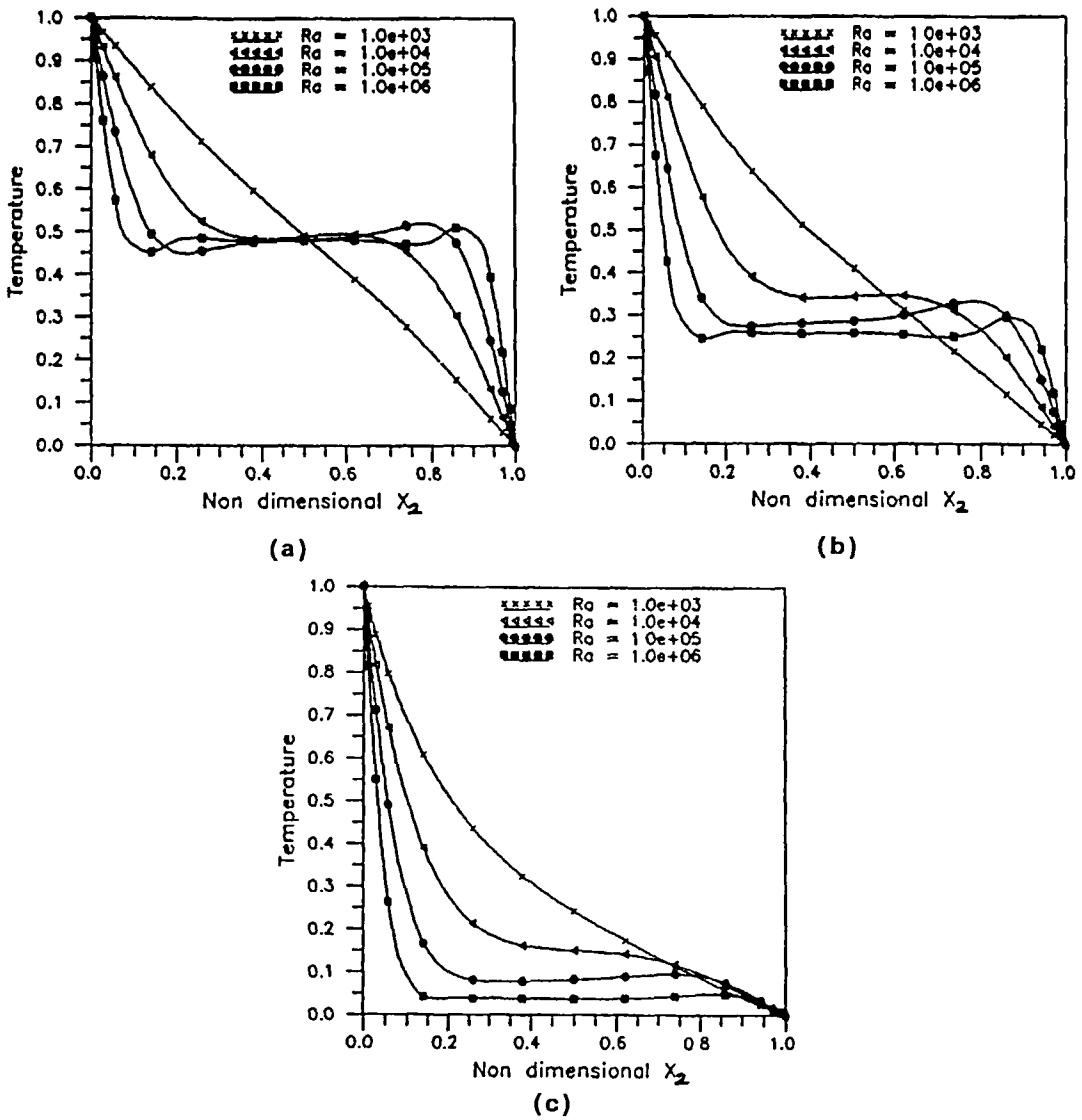

Figure 3 Comparison of temperature along the horizontal mid-plane of the cavity for different Rayleigh numbers: (a) $\lambda=0.999$, (b) $\lambda=0.500$, (c) $\lambda=0.091$

distribution are not symmetric about the mid-plane as was the case in a plane cavity. U_1 velocity, near the hot wall is much higher than that at the cold wall. Also the temperature gradient is much steeper near the hot wall due to less available area for heat transfer than near the cold wall. As a result, the boundary layer thickness is smaller near the hot wall. Consequently, the Nusselt number is higher than for a plane cavity. Further, from the temperature plots it is observed that the effect of curvature is to reduce the overall fluid core temperature. This is consistent with the findings of Woon-Shing Yeung[11]. *Figures 5a* and *5b* show the streamlines and isotherms for $\lambda=0.999$ and *Figures 6a* and *6b* show the same for $\lambda=0.091$. The streamlines and isotherms for $\lambda=0.999$ are very much same as those for a plane case[13,14]. For $Ra=10^5$ and 10^6 two secondary circulation zones appear in the core. This is supported by the presence

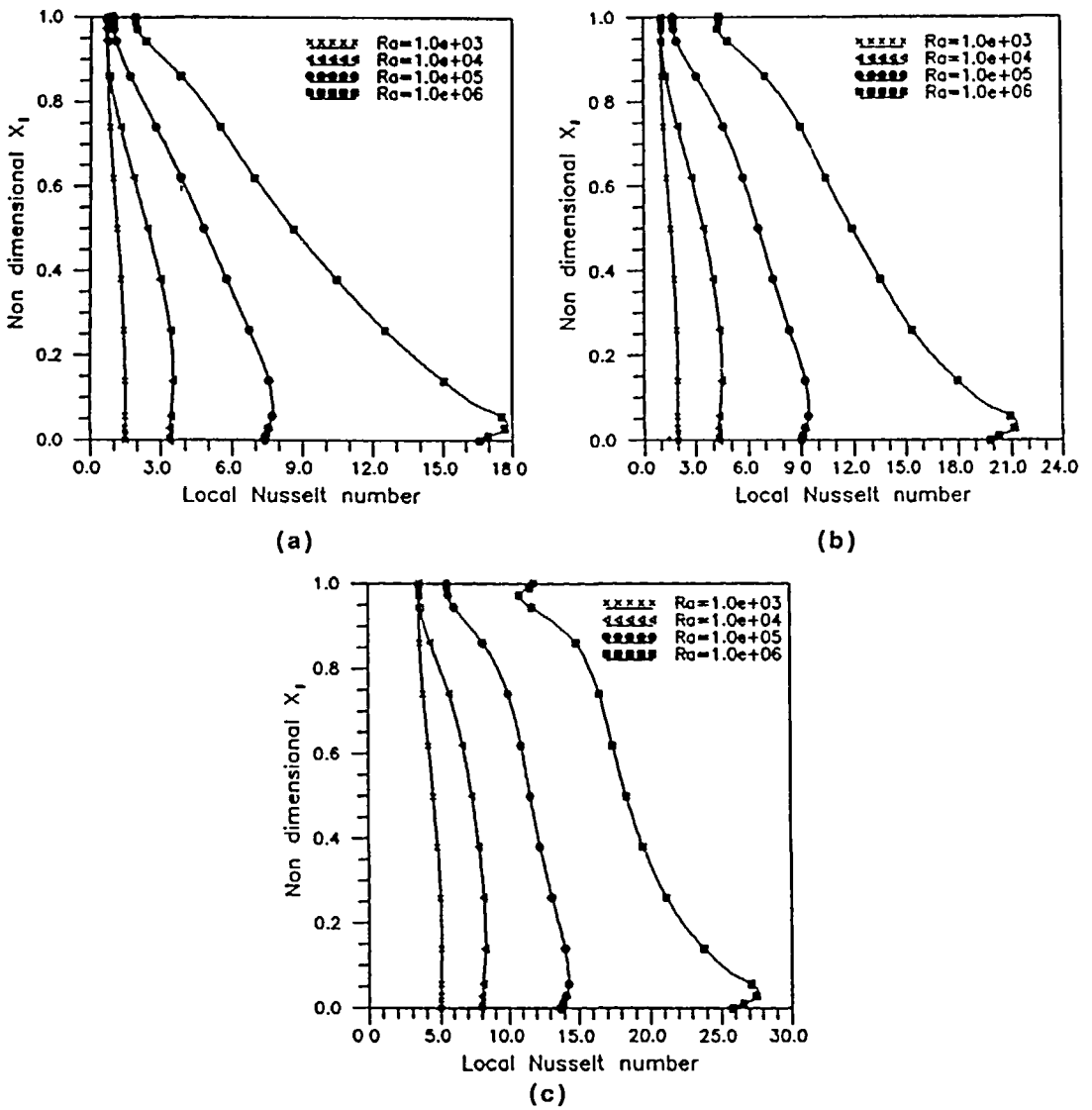

Figure 4 Comparison of Nusselt number distribution along the hot wall of the cavity for different Rayleigh numbers: (a) $\lambda=0.999$, (b) $\lambda=0.500$, (c) $\lambda=0.091$

of a small negative component of velocity just outside the boundary layer along the hot wall and a small positive component of velocity outside the cold wall boundary layer in *Figure 2*. The streamlines in the case of $\lambda=0.091$ (*Figure 6a*) are found to be more densely packed near the hot wall. This is also evident from *Figure 2c* in which the velocity along the hot wall is much higher than near the cold wall. Also the isotherms in the case of $\lambda=0.091$ (*Figure 6b*) are displaced towards the hot wall indicating that there is a much steeper temperature gradient near the hot wall than near the cold wall, a fact which was borne by *Figure 3c*.

Figures 7a and *7b* show the comparison of Nusselt number variation along the hot wall for $Ra=10^9$ and 10^6, with λ as a parameter. It is observed that the heat transfer rate along the hot wall significantly improves as λ is decreased. This is due to less available area near the hot wall

Table 1 Comparison of maximum vertical velocity for different *Ra* with available results

Rayleigh number	Maximum vertical component of velocity (U_{fmax})		
	de Vahl Davis[13]	Markatos and Pericleus[14]	Present results
10^3	3.697	3.593	3.65
10^4	19.620	19.440	19.65
10^5	68.590	69.080	69.50
10^6	219.360	221.800	226.00

Table 2 Comparison of average Nusselt numbers obtained in the present investigation with those in Reference 13

Rayleigh number	Average Nusselt number		
	Present results	Benchmark soln de Vahl Davis[13]	% age difference
10^3	1.1307	1.116	1.32
10^4	2.2894	2.242	2.11
10^5	4.6875	4.523	3.64
10^6	9.1443	8.928	2.42

as compared to the cold wall. *Figures 8a* and *8b* show the variation of local Nusselt number along the hot and the cold walls for $\lambda = 0.999$, 0.500 and 0.091 for $Ra = 10^9$ and 10^6. For $\lambda = 0.999$ the Nusselt number variation is almost symmetric on both the walls and the $\overline{Nu}$ values are close to each other as is evident from *Figure 8a* (i and ii). But as λ decreases the Nu_{max} along the hot and the cold walls differ more and more and hence the $\overline{Nu}$ values differ significantly. *Figures 9a* and *9b* show the variation of $\overline{Nu}$ for $Ra = 10^3$ and 10^6 along the hot and cold walls for different radius ratios (λ). It is evident that the $\overline{Nu}$ increases drastically as the radius ratio decreases from 0.999 to 0.091. These results follow the same trend as reported by de Vahl Davis and Thomas[7]. Figure 9 in Reference 7 shows the variation of $\overline{Nu}$ along the hot wall for different aspect ratios ranging from 5 to 20 and for different radius ratios. Since they did not present any results for aspect ratio of 1 it is not possible to obtain a comparison of the absolute values of $\overline{Nu}$ values of the present work with theirs. However, a qualitative agreement between the present results and those of References 7 and 8 could be observed.

CONCLUSIONS

A time and cost effective finite element code has been developed for studying the laminar natural convection in axisymmetric geometries and has been used to investigate into the heat transfer characteristics of an annular cavity. The code has been validated by considering a plane cavity (which is a limiting case of an annular cavity) for which published results are available. For the range of Rayleigh numbers and radius ratio investigated, it is observed that in an annular enclosure as the radius ratio is decreased (or the effect of radius of curvature is increased), the symmetry of the velocity field, temperature field and the Nusselt number distribution is lost. From the present investigation it is also found that, for fixed temperatures of the inner and outer walls of an annular cavity, the heat transfer coefficient increases as the radius ratio decreases.

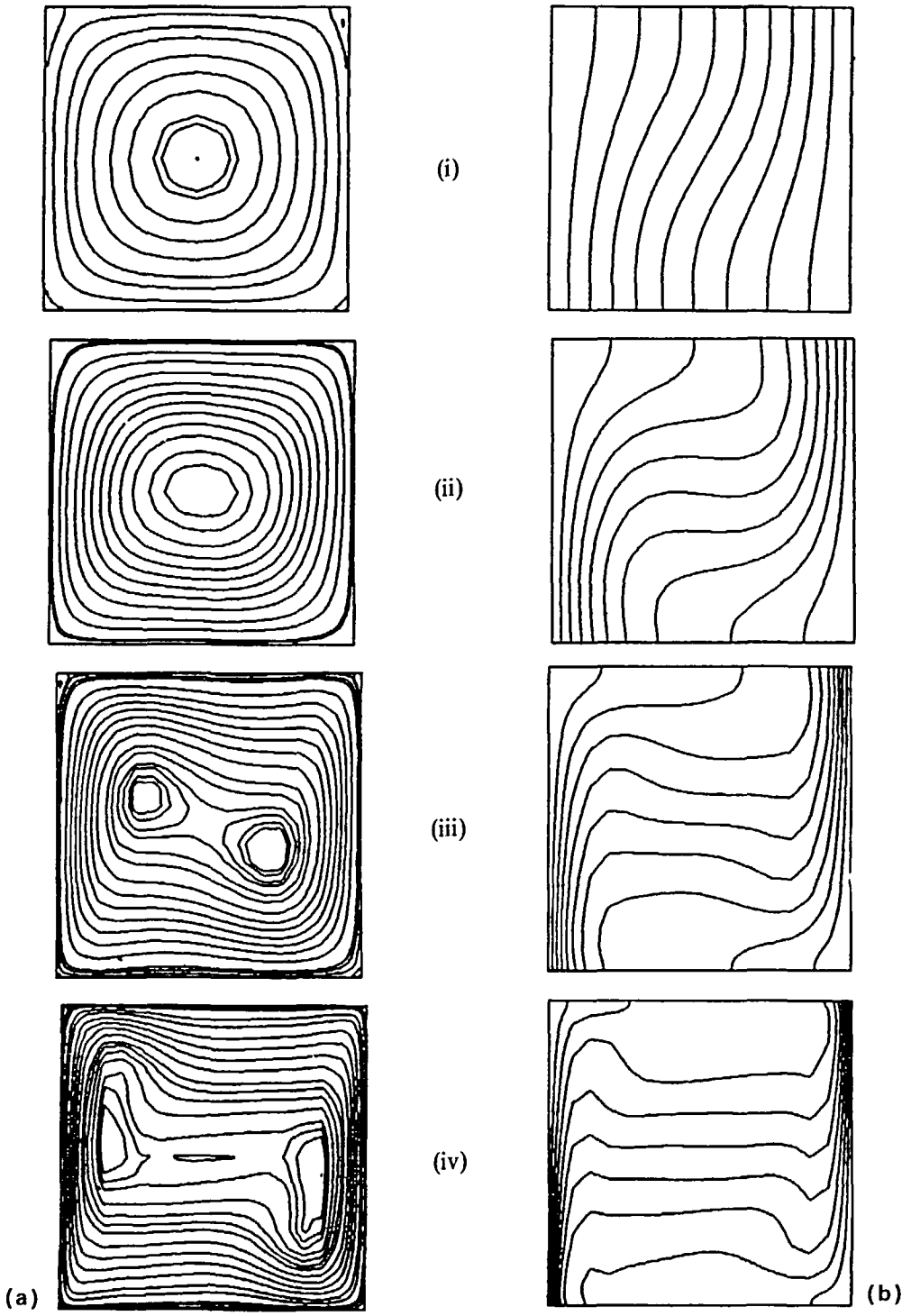

Figure 5 Streamlines and isotherms for radius ratio = 0.999. (a) Streamlines; (b) isotherms: (i) $Ra = 10^3$, (ii) $Ra = 10^4$, (iii) $Ra = 10^5$, (iv) $Ra = 10^6$

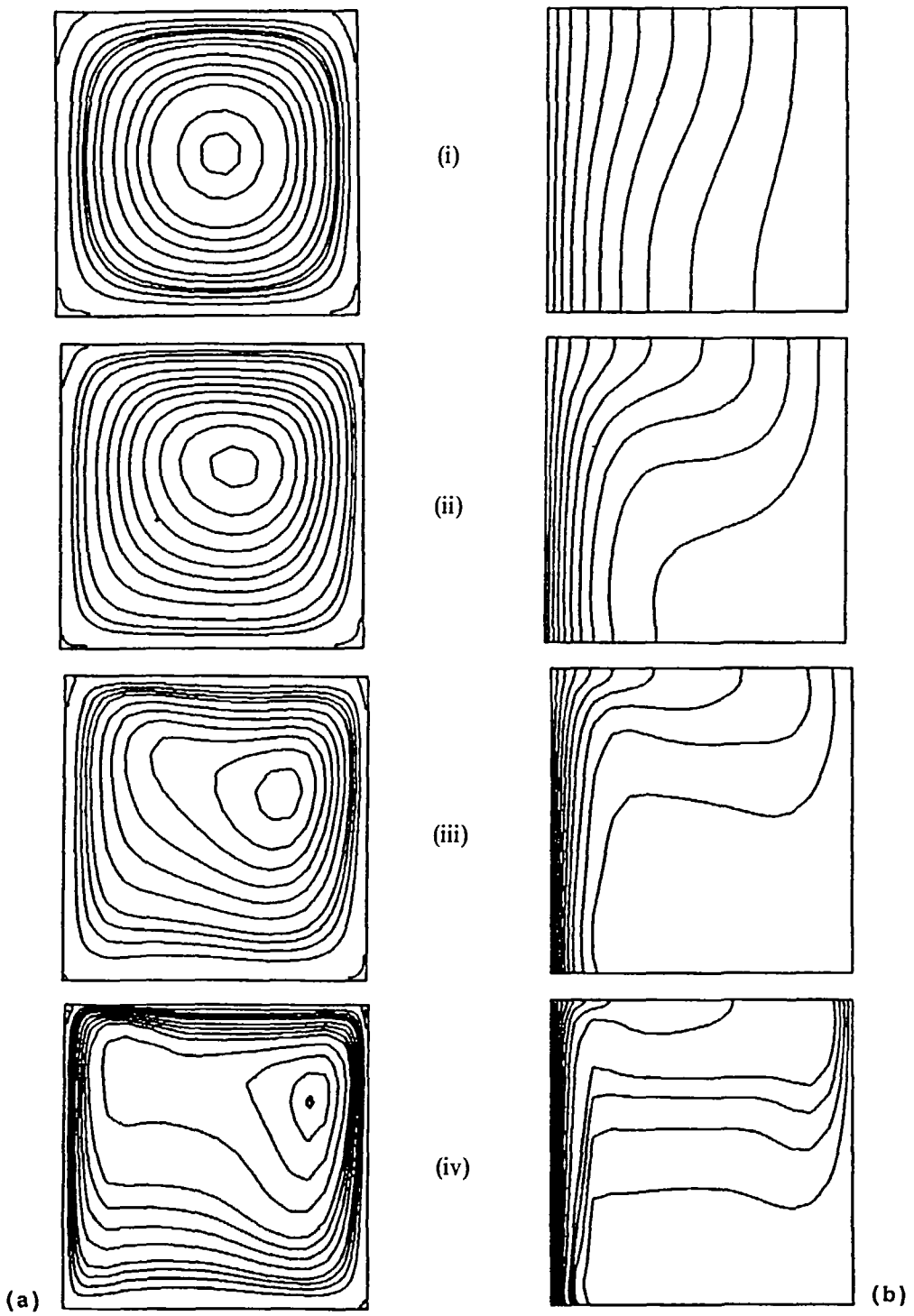

Figure 6 Streamlines and isotherms for radius ratio = 0.091. (a) Streamlines; (b) isotherms: (i) $Ra = 10^3$, (ii) $Ra = 10^4$, (iii) $Ra = 10^5$, (iv) $Ra = 10^6$

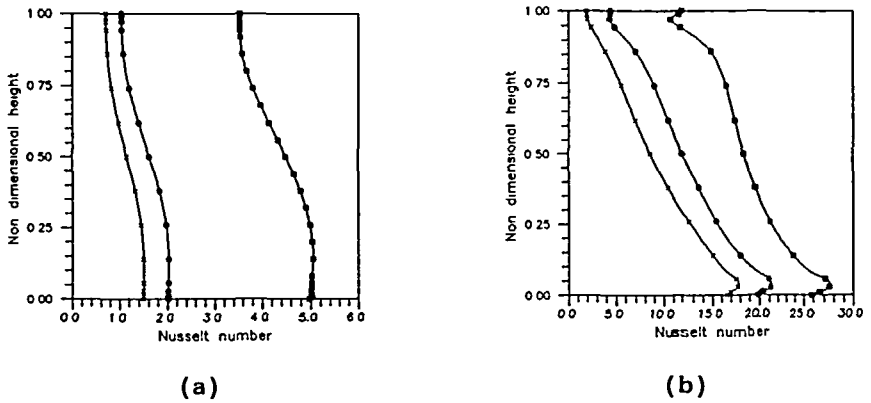

Figure 7 Comparison of Nusselt number variation along the hot wall of the cavity for different Rayleigh numbers with λ as parameter. (a) $Ra=10^3$; (b) $Ra=10^6$

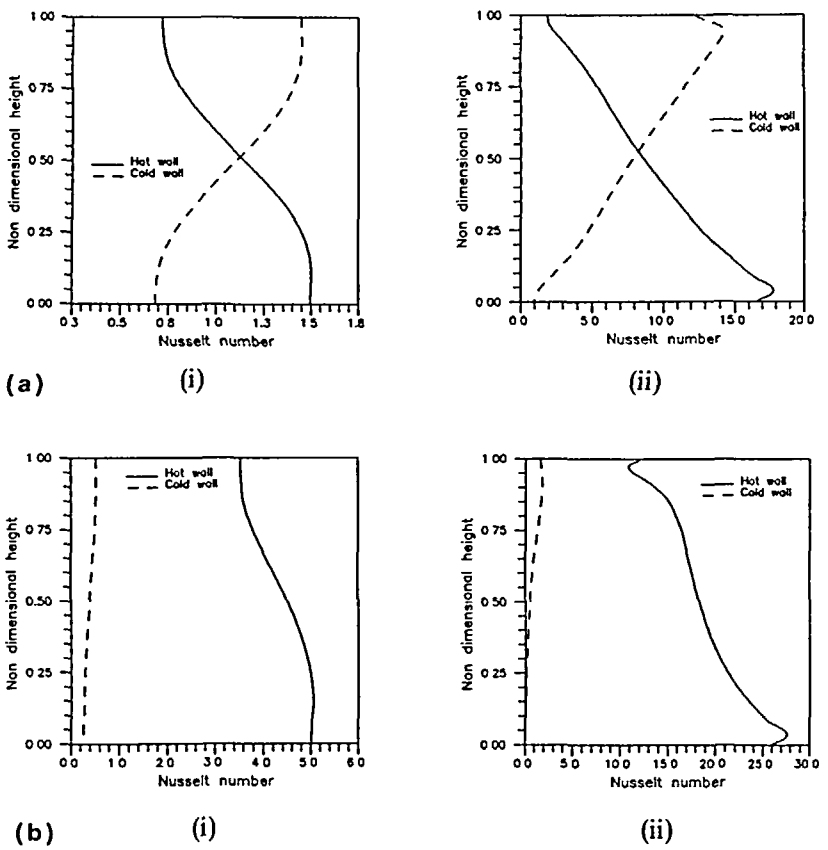

Figure 8 Comparison of Nusselt number variation along the hot and cold walls of the cavity for different values of λ. (a) $\lambda=0.999$; (b) $\lambda=0.091$: (i) $Ra=10^3$; (ii) $Ra=10^6$

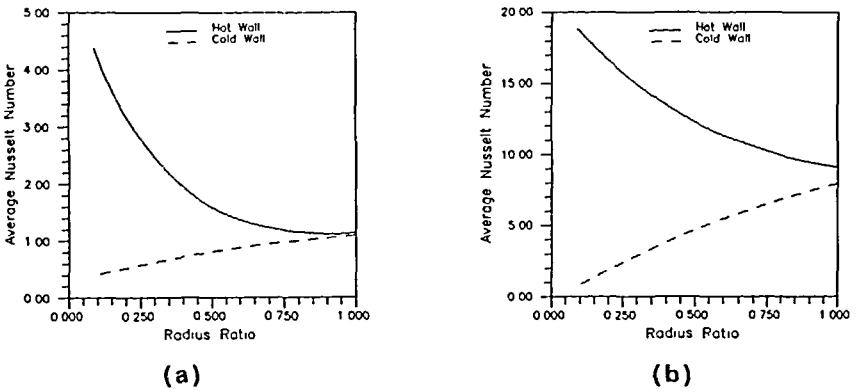

Figure 9 Variation of the average Nusselt number ($\overline{Nu}$) along the hot and cold walls of the cavity with radius ratio. (a) $Ra=10^3$; (b) $Ra=10^6$

ACKNOWLEDGEMENTS

The authors are grateful to the referees for their constructive suggestions which were helpful in the revision of the paper. The present work is carried out under the auspices of National Science Foundation, USA (Grant no: INT-8903119).

REFERENCES

1 Kakac, S., Aung, W. and Viskanta, R. (Eds.) *Natural Convection· Fundamentals and Applications*, Hemisphere, Washington, DC (1985)
2 Nagendra, H. R., Tirunarayanan, M. A. and Ramachandran, A. Free convective heat transfer in vertical annuli, *Chem. Eng. Sci.*, **25**, 605–610 (1970)
3 Keyhani, M., Kulacki, F. A. and Christensen, R. N. Free convection in a vertical annulus with constant heat flux at the inner wall, *ASME J. Heat Tranf.*, **105**, 454–459 (1983)
4 Bhushan, R., Keyhani, M., Christensen, R. N. and Kulacki, F. A. Correlation equations for free convection in a vertical annulus with constant heat flux on the inner wall, *ASME J. Heat Transf.*, **105**, 910–912 (1983)
5 Khan, J. A. and Kumar, R. Natural convection in vertical annuli: a numerical study for constant heat flux on the inner wall, *ASME J. Heat Transf.*, **111**, 909–915 (1989)
6 Fang, Z. and Paraschivoiu, I. A numerical study for natural convection in vertical annuli with high aspect ratio, *Proc. Seventh Int. Conf. Num. Meth. Thermal Problems, Stanford, CA*, Pineridge Press, Swansea (1991)
7 de Vahl Davis, G. and Thomas, R. W. Natural convection between concentric vertical cylinders, *High Speed Computing in Fluid Dynamics—Physics of Fluids Suppl. II*, pp. 198–207 (1969)
8 Wu-Shung Fu and Yi-Horng Jou, A transient natural convection in an annular enclosure, *Int. Commun. Heat Mass Transf.*, **18**, 373–384 (1991)
9 Le Quere, P. and Pecheux, J. Numerical simulations of multiple flow transitions in axisymmetric annulus convection, *J. Fluid Mech.*, **206**, 517–544 (1989)
10 Farouk, B., Ball, K. S. and Dixit, V. C. Aspect and radius ratio effects on natural convection in a vertical annulus, *9th Int. Conf. Heat Mass Transf. Jerusalem* (1990)
11 Woon-Shing Yeung, Analysis of natural convection in a closed vertical annulus, *Int. Commun. Heat Mass Transf.*, **16**, 445–455 (1989)
12 Segerlind, L. J. *Applied Finite Element Element Analysis*, John Wiley, New York (1984)
13 de Vahl Davis, G. Natural convection of air in a square cavity: a bench mark numerical solution, *Int. J. Num. Meth. Fluids*, **3**, 249–264 (1983)
14 Markatos, N. C. and Pericleus, K. A. Laminar and turbulent natural convection in an enclosed cavity, *Int. J. Heat Mass Transf.*, **27**, 755–772 (1984)